Editors' Suggestion | Featured in Physics

Direct Measurement of Hexacontatetrapole, $E6$ γ Decay from ^{53m}Fe

T. Palazzo,[1] A. J. Mitchell,[1,*] G. J. Lane,[1] A. E. Stuchbery,[1] B. A. Brown,[2] M. W. Reed,[1] A. Akber,[1] B. J. Coombes,[1] J. T. H. Dowie,[1] T. K. Eriksen,[1] M. S. M. Gerathy,[1] T. Kibédi,[1] T. Tornyi,[1] and M. O. de Vries[1]

[1]*Department of Nuclear Physics and Accelerator Applications, Research School of Physics, The Australian National University, Canberra, Australian Capital Territory 2601, Australia*

[2]*Department of Physics and Astronomy, and the Facility for Rare Isotope Beams, Michigan State University, East Lansing, Michigan 48824-1321, USA*

(Received 2 November 2022; accepted 9 February 2023; published 24 March 2023)

The only proposed observation of a discrete, hexacontatetrapole ($E6$) transition in nature occurs from the $T_{1/2} = 2.54(2)$-min decay of ^{53m}Fe. However, there are conflicting claims concerning its γ-decay branching ratio, and a rigorous interrogation of γ-ray sum contributions is lacking. Experiments performed at the Australian Heavy Ion Accelerator Facility were used to study the decay of ^{53m}Fe. For the first time, sum-coincidence contributions to the weak $E6$ and $M5$ decay branches have been firmly quantified using complementary experimental and computational methods. Agreement across the different approaches confirms the existence of the real $E6$ transition; the $M5$ branching ratio and transition rate have also been revised. Shell model calculations performed in the full fp model space suggest that the effective proton charge for high-multipole, $E4$ and $E6$, transitions is quenched to approximately two-thirds of the collective $E2$ value. Correlations between nucleons may offer an explanation of this unexpected phenomenon, which is in stark contrast to the collective nature of lower-multipole, electric transitions observed in atomic nuclei.

DOI: 10.1103/PhysRevLett.130.122503

First-order electromagnetic processes are the primary mechanism by which excited states in atomic nuclei relax, most often via single γ-ray emission. Since both initial- and final-state wave functions possess a well-defined spin (J) and parity (π), conservation laws impose a characteristic multipolarity ($\sigma\lambda$) for each discrete transition. Nature favors pathways that proceed via the lowest available multipole order; as such, $\Delta J = 1$, 2 transitions are prevalent in atomic and nuclear systems. However, situations arise in which the only available decay pathway is hindered by a larger angular-momentum-change requirement [1]. As the multipole order increases, the number of known cases decreases rapidly. For example, there are ≈1100 pure or mixed $\Delta J = 3$ ($E3$ or $M3$), ≈170 $\Delta J = 4$ ($E4$ or $M4$), and ≈25 $\Delta J = 5$ ($E5$ or $M5$) transitions reported in atomic nuclei.

Despite discovery of over 3000 different nuclides, only one claim of $\Delta J = 6$, or hexacontatetrapole, decay has been reported: the $J^\pi = 19/2^- \rightarrow J^\pi = 7/2^-$, $E6$ γ decay from ^{53m}Fe [2–5] (see Fig. 1 for details). Low-lying states in this nucleus can be understood in the $(f_{7/2})$ model space with an effective interaction derived from the energy-level spectra of ^{54}Co (^{53}Fe plus a proton) and ^{54}Fe (^{53}Fe plus a neutron) [4]. Isomerism of the $19/2^-$ level occurs due to its location relative to the other yrast states, i.e., those with the lowest excitation energy for a given spin and parity. The only alternate decay pathways to the $E6$ transition are the strongly hindered $M5$, $J^\pi = 19/2^- \rightarrow 9/2^-$ and $E4$, $J^\pi = 19/2^- \rightarrow 11/2^-$ transitions.

However, inconsistencies in γ-ray branching ratios and reduced transition rates are reported in the literature [2,3]. Although they are relatively rare, γ-ray "summing" events could be mistaken for the very weak, $E6$ decay; these occur when multiple γ rays are incident on the same detector within an unresolvable time window. It is even possible that no real $E6$ transition was observed in the prior work, and the feature at 3041 keV reported in the energy spectrum of Ref. [2] consists entirely of sum events. Despite their importance, a thorough and quantitative understanding of sum contributions was lacking [2,3].

This Letter reports the first direct confirmation of $E6$ γ decay in ^{53m}Fe using a novel combination of experimental, computational and Monte Carlo techniques that fully quantify the sum contributions; this confirms the highest multipole order ever observed. With a now-well-defined $E6$ transition strength, and revised values for the $M5$ and $E4$ γ decay, ^{53m}Fe provides a unique test of the nuclear shell model and our present understanding of high-multipolarity transitions within a single nuclear system. Comparison with theoretical shell model calculations performed in the full fp-model space shows, surprisingly, that low- and high-multipolarity transitions in atomic nuclei are fundamentally different in nature.

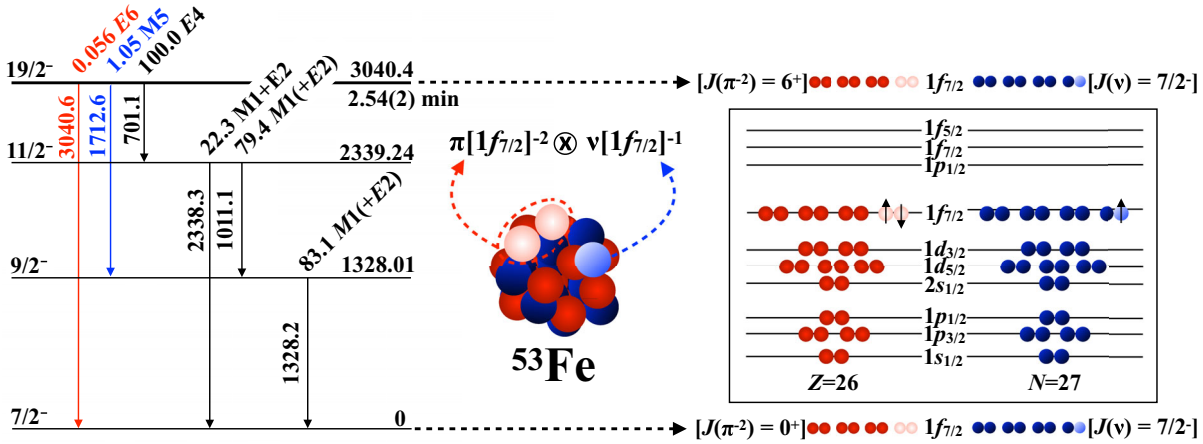

FIG. 1. Level scheme showing the energies (in keV) of excited states and γ-ray transitions observed in the decay of ^{53m}Fe [6], together with nucleon configurations that couple to form the $19/2^-$ isomer. The γ-ray intensities were determined in this Letter. Proton (neutron) particles are depicted by red (blue) solid spheres; proton (neutron) holes are shown as faded spheres. Coupling of the proton- and neutron-hole configurations leads to formation of the $19/2^-$ isomeric state at 3040 keV.

The experiments were performed at the Heavy Ion Accelerator Facility at the Australian National University. A 2-pnA beam of 50-MeV, ^{6}Li ions delivered by the 14UD Pelletron accelerator was incident on self-supporting targets of natural vanadium. Three separate, 10-mg/cm^2 thick targets were used; these were replaced periodically to suppress build up of long-lived activity. Excited states in ^{53}Fe were populated via the ^{51}V(^{6}Li, $4n$)^{53}Fe reaction. Other fusion-evaporation channels led to production of neighboring isotopes of iron, manganese, chromium, vanadium, titanium and scandium. Since many of these nuclides are stable against β decay, their prompt γ rays were easily separated from delayed decay of ^{53m}Fe via subtraction of suitable sections of the time-correlated data discussed below.

Relaxation of ^{53m}Fe was studied via γ-ray spectroscopy using the CAESAR array of Compton-suppressed High-Purity Germanium (HPGe) detectors [7]. Of the nine detectors used, six were fixed in the vertical plane, perpendicular to the beam axis and ≈12 cm from the target. The remaining three, in the horizontal plane, were on rail systems allowing their radial position to be moved. The detector-suppressor assemblies were retracted such that the front collimator that defines the detector illumination was moved from ≈8.5 to ≈12 cm from the target between measurements, reducing the exposed solid angle by approximately a factor of 2. These are referred to as the "near" and "far" geometries, respectively, and discussed quantitatively in the text below. Standard γ-ray sources of ^{152}Eu and ^{56}Co were used for energy and absolute detection-efficiency calibrations.

A continuous ^{6}Li beam irradiated the target for 7.5 min (approximately three half-lives of ^{53m}Fe), after which the beam was intercepted and decay of the isomer was observed for 20 min (approximately eight half-lives). A custom-made counter, with an oscillator that can be driven at various well-defined frequencies, was used in conjunction with the CAESAR data acquisition system to time-stamp individual γ-decay events across many repeating irradiation-decay cycles. Observation of intense 701-, 1011-, 1328- and 2338-keV γ rays confirmed production of ^{53m}Fe.

The bulk of nuclei produced in the reactions have much longer lifetimes than ^{53m}Fe. Subtracting the second 10 minutes of the collection cycle from the first 10 min resulted in a much cleaner energy spectrum that strongly enhances the peak-to-total ratio for ^{53m}Fe decay, while only sacrificing ≈12% of the total ^{53m}Fe data collected. The time spectrum of collected events, as well as the total γ-ray and time-subtracted γ-ray energy spectra are presented in Fig. 2. Gamma rays from the decay of ^{53m}Fe have been labeled by their energy in keV. The remaining γ rays have been identified as arising from decay of ^{75m}Ge ($T_{1/2} = 48$ s), and β decay of ^{51}Ti ($T_{1/2} = 346$ s), ^{53}Fe (ground state, $T_{1/2} = 510$ s), ^{52}V ($T_{1/2} = 208$ s), ^{20}F ($T_{1/2} = 11$ s), and ^{28}Al ($T_{1/2} = 134$ s).

Total yields of γ rays from ^{53m}Fe decay, measured in both geometries, are provided in Table I of Ref. [8]. In addition to the real $E6$ transition reported in this Letter, ^{53m}Fe exhibits three alternate decay pathways to the ground state (refer to Fig. 1 for details). Each individual cascade presents a potential summing contribution (S_i) to the true 3041-keV γ-ray intensity (I_γ) that requires careful consideration. The observed full-energy peak yield (Y_γ) is given by

$$Y_\gamma = I_\gamma + \Sigma S_i, \tag{1}$$

where the sum is over each possible multitransition cascade that connects the level to the ground state. While the real

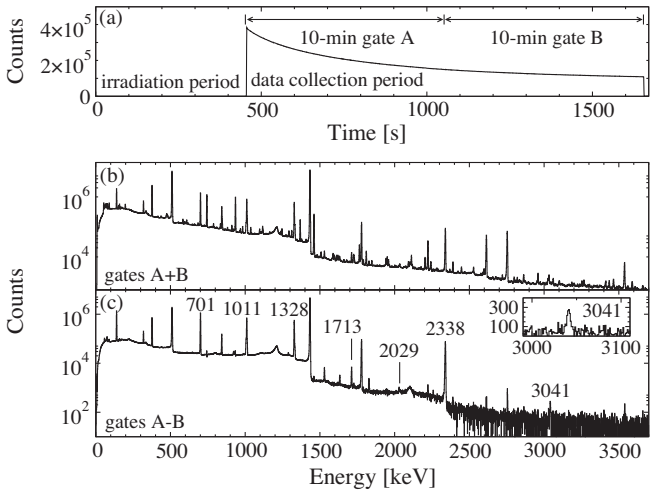

FIG. 2. (a) Time spectrum from the ADC clock recorded with each γ-ray event illustrating the irradiation and out-of-beam collection period split into two parts, gates A and B. Lower panels show (b) the total γ-ray spectrum recorded (gate A plus gate B) and (c) the subtracted spectrum (gate A minus gate B) described in the text. The inset spectrum is on a linear scale and expands the region near the 3041-keV, $E6$ transition.

1713-, 2338-, and 3041-keV full-energy peaks are all expected to contain individual sum contributions, an additional peak observed at 2029 keV in Fig. 2 is entirely composed of sum events (701 keV + 1328 keV).

Experimental and computational methods were adopted to quantify the sum-coincidence component in each of these measured full-energy peak yields. Full details of the methods and their results are described in Refs. [8,9]; a brief explanation of each method is provided here: (i) *Experimental*: The measured yield of the 2029-keV full-energy sum peak, which can *only* occur though summing, can be scaled to estimate the sum-coincidence components of the other transitions while accounting for detection efficiencies and angular correlations. (ii) *Geometric*: Sum-coincidence events can be directly inferred by considering changes in counting efficiency between the near and far detector geometries. (iii) *Computational*: The sum contribution to $Y_\gamma(3041\ \mathrm{keV})$ can be estimated from measured γ-ray intensities, detection efficiencies, and angular correlations by solving the set of equations that govern the different sum contributions. (iv) *Monte Carlo*: A Monte Carlo simulation was developed to model the γ decay of ^{53m}Fe and evaluate summing contributions expected with the CAESAR array.

Consistency between the various approaches across both detector geometries gives confidence in the deduced branching ratios. Therefore, the analysis confirms that the $E6$ transition is real, and enables a firm measurement of its decay branching ratio for the first time.

Transition strengths for the $E4$, $M5$, and $E6$ decays were calculated using the new branching ratios derived from results of the experimental method; they are presented in Table I. These have been determined using the adopted $19/2^-$ state lifetime of $T_{1/2} = 2.54(2)$ min [6] and theoretical internal conversion coefficients; values for $L = 1$–5 were calculated using BRICC [10], while for $L = 6$ it was calculated directly using the RAINE code [11]. Intensities reported by Black *et al.* [2,3], and transition strengths determined using the relative intensities of Ref. [3] are included for comparison. We confirm the reported values for $E4$ decay, however, the competing $M5$ branching ratio and transition strength were found to be ≈20% lower. Notably, the branching ratios of transitions depopulating the state at 2339 keV were also found to be significantly different to those of Black *et al* [3].

To gain microscopic understanding of the high-multipolarity transitions in ^{53m}Fe, shell model calculations were performed with the NuShellX code [12]. For comparisons between theory and experiment, it is useful to consider the reduced matrix element, $\mathcal{M}_p$, which is related to the reduced transition strength by

$$B(E\lambda; J_i \to J_f) = \frac{\mathcal{M}_p^2}{(2J_i + 1)}, \tag{2}$$

TABLE I. Summary of adopted level and γ-ray energies, transition multipolarities, newly measured relative intensities (taking sum-coincidence events into account), and deduced transition strengths for the $E4$, $M5$, and $E6$ measured in this Letter quoted in units of Weisskopf units (W.u), as well as $e^2\,\mathrm{fm}^{2\lambda}$ for the $E4$ and $E6$ transitions and $\mu_N^2\,\mathrm{fm}^{2\lambda-2}$ for the $M5$. The half-life of the $J^\pi = 19/2^-$ isomer is 2.54(2) min [6]. Conflicting relative intensities quoted in Table 1 of Ref. [2] and Table III of Ref. [3] are provided for reference. Transition strengths calculated using the branching ratios of Ref. [3] are also provided for comparison with those of the present work.

E_{Level}	E_γ	σL	I_γ			$B(\sigma\lambda)$ (W.u)		$B(\sigma\lambda)$ ($e^2\mathrm{fm}^{2\lambda}$, $\mu_N^2\,\mathrm{fm}^{2\lambda-2}$)	
Ref. [6]	Ref. [6]	Ref. [6]	This Letter	Ref. [2]	Ref. [3]	This Letter	I_γ([3])	This Letter	I_γ(Ref. [3])
3040.4	701.1(1)	$E4$	≡100	≡100	≡100	0.2593(21)	0.2587(21)	$6.46(5) \times 10^2$	$6.44(6) \times 10^2$
	1712.6(3)	$M5$	1.05(5)	0.7(1)	1.3(1)	4.34(21)	5.4(4)	$3.31(16) \times 10^5$	$4.1(3) \times 10^5$
	3040.6(5)	$E6$	0.056(17)	0.020(5)	0.06(1)	0.42(12)	0.45(8)	$2.61(81) \times 10^5$	$2.8(5) \times 10^5$
2339.24	1011.2(2)	$M1(+E2)$	79.4(3)	86(9)	86(9)				
	2338.3(5)	$M1 + E2$	22.3(2)	13(2)	13(2)				

where $\mathcal{M}_p$ is further separated into its proton ($\mathcal{A}_p$) and neutron ($\mathcal{A}_n$) contributions:

$$\mathcal{M}_p = \mathcal{A}_p \cdot \varepsilon_p + \mathcal{A}_n \cdot \varepsilon_n. \quad (3)$$

Typically, $\mathcal{A}_p$ and $\mathcal{A}_n$ are calculated to account for configuration mixing within the major shell, while effective nucleon charges are introduced to account for cross-shell mixing. Thus $\varepsilon_{p,n} = e_{p,n} + \delta_{p,n}$, where $e_{p,n}$ are bare nucleon charges and $\delta_{p,n}$ are core-polarization charges.

Calculations were performed within a restricted $(f_{7/2})^{13}$, and full fp model space with two commonly used Hamiltonians, GFPX1A [13], and KB3G [14]. Excited-state energies were in good agreement with the adopted values [6]; for example, the energies of the $19/2^-$, $11/2^-$, and $9/2^-$ states calculated with the GFPX1A interaction have a root-mean-squared (rms) deviation of 169 keV. Matrix elements for the electromagnetic transitions are sensitive to the rms radius of the $0f_{7/2}$ orbit, and with harmonic oscillator radial wave functions they scale approximately with b^λ, where b is the oscillator length parameter. Spherical Skyrme Hartree-Fock calculations, with Skx [15] and Sly4 [16] interactions, were used to determine the $0f_{7/2}$ orbital rms radius. The Skx $0f_{7/2}$ rms radius was reproduced by the harmonic oscillator model with $b = 1.937$ fm. This parameter is approximately 3% larger for Sly4, which represents the theoretical uncertainty in the rms radius. The matrix elements, therefore, have uncertainties of 18%, 15%, and 12% for the calculated $\lambda = 6$, 5, 4 matrix elements, respectively.

The full set of results is provided in Table II of Ref. [8], and average values of both fp-shell calculations are summarized and compared to experiment in Table II in this Letter. Results of the $(f_{7/2})^{13}$ calculations are similar to those in Ref. [17]. Surprisingly, matrix elements obtained in the full fp model space are almost a factor of 2 smaller than the restricted-basis values. This is unusual, since strong $\lambda = 2$ transitions are generally enhanced in the full fp space with respect to the restricted one. This behavior comes about because the high-λ transitions are dominated by the $0f_{7/2}$ orbital; in the larger space, the matrix elements are diluted by mixing of the $0f_{7/2}$ component with $1p$ orbitals, which cannot contribute to the high-multipolarity transitions; in contrast, the $1p$ orbitals contribute to and enhance $\lambda = 2$ transition strength.

A remarkable aspect of these high-multipolarity transitions is that they are dominated by their proton component. This, again, is in contrast to strong $B(E2)$ transitions, in which the proton and neutron components are typically observed to be similar. For this reason, the isoscalar $E2$ effective charge is best determined with, for example, the empirical value of $\varepsilon_p + \varepsilon_n = 2.0$ obtained in Ref. [18]. The separate proton and neutron $E2$ effective charges can only be obtained in special cases. An example is the $A = 51$ mirror nuclei system [19], where values of $\varepsilon_p \approx 1.15$ and $\varepsilon_n \approx 0.80$ were obtained from the measured $E2$ transition data.

The calculated proton and neutron contributions and experimental matrix elements, presented in Table II, can be used with Equation (3) to obtain effective proton charges for the high-multipolarity electric transitions. For the small neutron component, $\varepsilon_n = 0.5$ is adopted [20]. The results obtained are: $\varepsilon_p = 0.62(13)$ for $\lambda = 6$; and $\varepsilon_p = 0.64(6)$ for $\lambda = 4$; if a value of $\varepsilon_n = 0$ is used instead, $\varepsilon_p = 0.65(13)$ and $\varepsilon_p = 0.80(7)$ are found for $\lambda = 6$ and $\lambda = 4$, respectively. These results are presented in Fig. 3, along with the value of $\varepsilon_p = 1.15$ for $\lambda = 2$ from Ref. [19], which has an assumed uncertainty of 5%.

Effective charges are evaluated by considering the coupling of valence nucleons to particle-hole excitations of the core. Whether based on perturbation theory or the particle-vibration concepts of Bohr and Mottelson [21], there is a choice of—and sensitivity to—the residual particle-hole interaction adopted in the calculation. Core-polarization contributions for all λ values were calculated for seven different interactions in Ref. [20]. The results of

TABLE II. Theoretical values of proton and neutron contributions to the $E4$, $M5$, and $E6$ matrix elements ($\mathcal{A}_{p,n}$) calculated in the full fp model space, discussed in the text. Uncertainties in the calculated matrix elements are $\pm(18, 15, 12)\%$ for $\lambda = (6, 5, 4)$, respectively. For the $M5$ transition, $\mathcal{M} = (\mathcal{A}_p + \mathcal{A}_n)$. Experimental matrix elements ($\mathcal{M}_p^{\text{expt.}}$) are determined from this Letter.

σL	$\mathcal{A}_p \times 10^3$	$\mathcal{A}_n \times 10^3$	$\mathcal{M} \times 10^3$	$\mathcal{M}_p^{\text{expt.}} \times 10^3$
$E4$	0.142(17)	0.045(7)	⋯	0.1137(5)
$M5$	5.09(76)	−0.11(2)	4.98(76)	2.57(6)
$E6$	3.52(63)	0.22(4)	⋯	2.29(35)

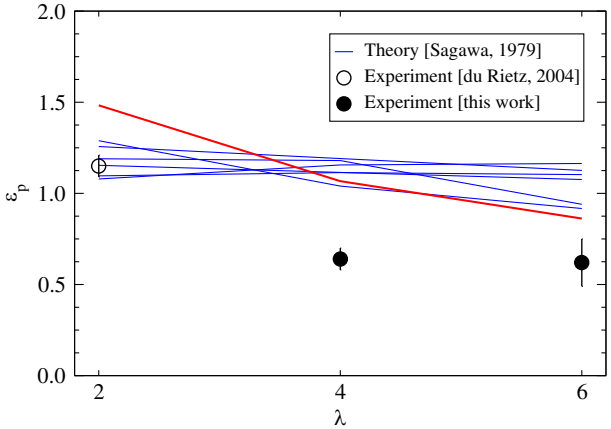

FIG. 3. Proton effective charges calculated for $\lambda = 2$, 4, and 6 with seven different interactions (red and blue lines) [20] compared to experimental values for $\lambda = 2$ (open circle) [19] and $\lambda = 4$, 6 (closed circles) from this work.

these calculations, summarized in Table I of Ref. [20], are compared to empirical values for $\lambda = 2, 4, 6$ in Fig. 3. The one that adopts Wigner-type interactions, shown in red, has a trend which is closest matched to experiment. However, while there is excellent agreement for $\lambda = 2$, all of the theoretical results are too large for $\lambda = 4$ and $\lambda = 6$.

The $E6$ matrix element within the $(0f_{7/2})^{13}$ configuration can be written as a product of two $0f_{7/2}$ spectroscopic amplitudes for one-proton removal times the single-particle $E6$ matrix element. Cross sections from $(e, e'p)$ data are also proportional to the product of two $0f_{7/2}$ spectroscopic amplitudes; these are quenched by about a factor of 2 compared to those calculated in the fp model space [see, e.g., Ref. [22] for $^{51}\mathrm{V}(e, e'p)^{50}\mathrm{Ti}$]. This is interpreted as a "dilution" of the fp part of the wave function due to short- [23,24] and long-range [25] correlations that go beyond the fp model space. This phenomenon is observed more broadly across the nuclear landscape [26,27] and cross sections extracted from nucleon transfer-reaction data are also known to be quenched by a similar magnitude [28]. The similarities suggest that quenching of the $E6$ matrix element observed in this Letter and quenching of $(e, e'p)$ cross sections are connected. Ultimately, any model that is used to understand the quenching of nucleon-removal cross sections should be extended to include calculations of electromagnetic matrix elements.

Since matrix elements of single-particle operators can be expanded in terms of the overlap integrals between eigenstates of a system with A nucleons and one of mass $(A-1)$ [29], high-multipole transitions appear to provide a sensitive probe of single-particle features of atomic nuclei. Further theoretical investigation into the high-multipolarity matrix elements, that includes such correlations, is therefore necessary.

In summary, experimental observation of an $E6$ transition in $^{53}\mathrm{Fe}$ is unambiguously confirmed by identifying and removing sum-coincidence contributions with three distinct methods that are in mutual agreement. Transition strengths for the high-multipolarity transitions from the 2.54(2)-min, $J^\pi = 19/2^-$ isomer have been determined from the newly measured branching ratios. In the fp model space, the $E6$ strength comes mainly from the dominant $(0f_{7/2})^{13}$ configuration. When this mixes with the many other fp configurations, the $(0f_{7/2})^{13}$ configuration becomes "diluted" and the total $E6$ matrix element decreases by about a factor of 2 in our calculations. The negative effective charge obtained for the full fp model space for $E6$ could be connected as a further dilution relative to the "exact" wave function that goes beyond the fp model space. Connection of the reduction of $(e, e'p)$ cross sections compared to those calculated in the fp model space was also discussed.

The authors are grateful for excellent support from technical staff of the Department of Nuclear Physics and Accelerator Applications, ANU, and the Australian Heavy Ion Accelerator Facility. We thank J. Heighway for preparing targets for these experiments. This work was supported by the Australian Research Council Grants No. DP170101673 and No. DP170101675, the International Technology Center Pacific (ITC-PAC) under Contract No. FA520919PA138, and NSF Grant No. PHY-2110365. A. A., B. J. C., J. T. S. D., M. S. M. G., and T. P. acknowledge support of the Australian Government Research Training Program. Support for the ANU Heavy Ion Accelerator Facility operations through the Australian National Collaborative Research Infrastructure Strategy program is acknowledged. Figure 1 in this Letter was created using the LevelScheme scientific figure preparation system [30].

*aj.mitchell@anu.edu.au

[1] P. Walker and G. D. Dracoulis, Nature (London) **399**, 35 (1999).
[2] J. N. Black, W. C. McHarris, and W. H. Kelly, Phys. Rev. Lett. **26**, 451 (1971).
[3] J. N. Black, W. C. McHarris, W. H. Kelly, and B. H. Wildenthal, Phys. Rev. C **11**, 939 (1975).
[4] D. Geesaman, Ph.D. thesis, State University of New York, Stony Brook, NY, 1976.
[5] D. F. Geesaman, R. L. McGrath, J. W. Noé, and R. E. Malmin, Phys. Rev. C **19**, 1938 (1979).
[6] H. Junde, Nucl. Data Sheets **110**, 2689 (2009).
[7] G. D. Dracoulis and A. P. Byrne, Annual Report No. ANU-P/1052, 1989.
[8] See Supplemental Material at http://link.aps.org/supplemental/10.1103/PhysRevLett.130.122503 for details pertaining to the sum-event evaluation methods.
[9] T. Palazzo, Master's thesis, The Australian National University, Canberra (Australia), 2017, 10.25911/5d6510089d770.
[10] T. Kibédi, T. W. Burrows, M. B. Trzhaskovskaya, P. M. Davidson, and C. W. Nestor, Jr., Nucl. Instrum. Methods Phys. Res., Sect. A **589**, 202 (2008).
[11] I. Band, M. Trzhaskovskaya, C. Nestor, P. Tikkanen, and S. Raman, At. Data Nucl. Data Tables **81**, 1 (2002).
[12] B. Brown and W. Rae, Nucl. Data Sheets **120**, 115 (2014).
[13] M. Honma, T. Otsuka, B. A. Brown, and T. Mizusaki, Eur. Phys. J. A **25**, 499 (2005).
[14] A. Poves, J. Sánchez-Solano, E. Caurier, and F. Nowacki, Nucl. Phys. **A694**, 157 (2001).
[15] B. A. Brown, Phys. Rev. C **58**, 220 (1998).
[16] B. Brown, R. Radhi, and B. Wildenthal, Phys. Rep. **101**, 313 (1983).
[17] D. H. Gloeckner and R. D. Lawson, Phys. Rev. C **11**, 1832 (1975).
[18] M. Honma, T. Otsuka, B. A. Brown, and T. Mizusaki, Phys. Rev. C **69**, 034335 (2004).
[19] R. du Rietz *et al.*, Phys. Rev. Lett. **93**, 222501 (2004).
[20] H. Sagawa, Phys. Rev. C **19**, 506 (1979).

[21] A. Bohr and B. R. Mottelson, *Nuclear Structure* (World Scientific Publishing Company, Singapore, 1998).
[22] J. W. A. den Herder, J. A. Hendriks, E. Jans, P. H. M. Keizer, G. J. Kramer, L. Lapikás, E. N. M. Quint, P. K. A. de Witt Huberts, H. P. Blok, and G. van der Steenhoven, Phys. Rev. Lett. **57**, 1843 (1986).
[23] H. Müther, A. Polls, and W. H. Dickhoff, Phys. Rev. C **51**, 3040 (1995).
[24] W. H. Dickhoff, J. Phys. G **37**, 064007 (2010).
[25] C. Barbieri, Phys. Rev. Lett. **103**, 202502 (2009).
[26] L. Lapikás, Nucl. Phys. **A553**, 297 (1993).
[27] G. Kramer, H. Blok, and L. Lapikás, Nucl. Phys. **A679**, 267 (2001).
[28] B. P. Kay, J. P. Schiffer, and S. J. Freeman, Phys. Rev. Lett. **111**, 042502 (2013).
[29] T. Berggren, Nucl. Phys. **72**, 337 (1965).
[30] M. Caprio, Comput. Phys. Commun. **171**, 107 (2005).